Liquid Micro-jet Array Impingement Boiling on a Micro-structured Surface

Avijit Bhunia, Ya-Chi Chen, and C. L. Chen
Teledyne Scientific Company 1049 Camino Dos Rios Thousand Oaks, CA 91360, U.S.A.
E-mail: abhunia@teledyne.com Tel: (805) - 373 - 4348

ABSTRACT

This article reports the role of micro-structured surfaces on phase change heat transfer due to impingement of a liquid micro-jet array. Experiments are conducted with an array of sixteen free surface DI water jets, each 125 μm diameter, at two different jet Reynolds number conditions of 1012 and 1747. A systematic, parametric study is carried out with eight different micro-structure patterns, all square cross-section micro-studs, by varying stud size, height, spacing, and stud arrangement (in-line and staggered array of studs). The structures are fabricated over a base area of 0.0001 m^2 (1 cm^2). In general, compared to the plain base surface, all the micro-structures improve impingement boiling heat transfer. The performance enhancement occurs in all regimes of boiling: at the onset, fully developed nucleate boiling and the critical heat flux (CHF). The optimal microstructure shows up to 78% increase in CHF compared to the plain surface. Heat flux in excess of 1000 Watts/cm^2 is demonstrated. The results are explained in light of the three distinct roles played by the micro-structures: (a) additional surface area, (b) additional bubble nucleation sites, and (c) obstruction to spreading of the high-speed, thin liquid film on the impingement surface.

NOMENCLATURE

A_{base}	Base area of the impingement surface (1 cm^2)
A_{total}	Total surface area of a micro-structured surface
C_p	Specific Heat. Subscript "l" and "v" respectively for liquid and vapor
CHF	Critical Heat Flux. Subscript A_{base} — calculated over 1 cm^2 base plate area, subscript A_{total} — calculated over total area of the micro-structured surface
d	Depth/ thickness of the base plate
D_j	Jet diameter at the outlet of the orifice
H	Stud height
i	Input current to the cartridge heaters
k	thermal conductivity. Subscript "s" for the solid (base plate) material or copper in this case
N_j	Number of jets
N_s	Number of studs
P	Jet/ orifice pitch
Q_{Abase}	Heat flux calculated over the base area = Q_H/A_{base}
Q_{Atotal}	Heat flux calculated over the total area = Q_H/A_{total}
Q_H	Power dissipated = $V.i - Q_{loss}$
Q_{loss}	Heat loss from the cartridge heater assembly
Q_L	Total liquid flow rate from all the jets
Re_j	Reynolds number of individual jets = $V_j D_j/ \nu = 4Q_L/(N_j \pi D_j \nu)$
S	Spacing between two micro-studs
t_f	Thickness of the liquid film formed on the heater (target) surface due to free surface liquid jet impingement

T_{bp}	Base plate temperatures. Subscript "*av*" for average value of multiple (1 through 4) measurements
T_L	Coolant liquid temperature, subscript "*in*" for inlet and "*out*" for outlet
$T_{s,av}$	Average temperature at the impingement surface
T_{sat}	Saturation or boiling temperature of the coolant liquid
V	Input voltage in the cartridge heaters
V_j	Average free surface jet velocity at the exit of the orifice plate
w	Stud width/length (square cross-section)
z	Impingement distance between jet source (orifice) and target surface
ΔT_{sab}	Sub-cooling of the impinging liquid $= T_{sat} - T_{L,in}$
ΔT_{sap}	Superheat in impingement boiling $= T_{s,av} - T_{sat}$
ε	Heat transfer effectiveness of micro-structured surface
ε_{ph}	Phase change effectiveness
ν	Kinematic viscosity of the liquid (DI water)
ρ	Density of liquid (DI water)

1. INTRODUCTION

Power density of both consumer and military electronics has steadily increased in recent years with more power and additional functionalities in reduced device footprint areas. The dissipation power density has also grown at a proportional rate, reaching hundreds or even thousands of Watts/cm^2 level. Heat removal at this high heat flux, along with the constraints of device and ambient temperature requirement dictated by the device reliability and the operating environment, is a serious challenge. With conventional cooling techniques, an electronics designer is forced to de-rate the output power of the devices or operate them at part of the duty cycle. The necessity of high heat flux cooling techniques, particularly involving phase change heat transfer, has been widely emphasized over the past decade, e.g. [1]. Several thermal roadmaps were created leading to an intense research in micro-scale, phase change-based cooling techniques, such as micro-channel flow, jet, droplet or spray impingement. This article focuses on one such high-heat-flux cooling technique: liquid micro-jet array impingement.

Research on liquid jet impingement heat transfer dates back over two decades. Multiple impingement configurations, such as free surface, submerged, confined or semi-confined jet, with cylindrical (round) or 2-D (slot) jet, and a single jet or jet array, have been considered. The topic has also been reviewed in great detail, both for single phase [2, 3, 4], and phase change (boiling) [5] heat transfer. In more recent years the focus has shifted from mm-scale (diameter) to micro-scale jets. Micro-scale jets are mostly laminar (jet Reynolds number Re_j typically less than ~2000), and are expected to form thinner liquid film on the impingement surface compared to the mm-scale jets. A significant amount of recent literature has investigated micro-jet impingement heat transfer, but mostly impingement on a plain (smooth) surface. For the sake of brevity, we refrain from citing these literatures, and only refer to those directly related to the current topic, i.e. the role of a structured surface on jet impingement boiling. Literature is rather scarce on this topic. Wadsworth and Mudawar [6] considered a free surface, 2-D (rectangular or slot) jet (250–500 μm wide) impingement on a heater surface with micro-studs and micro-grooves (~300 μm wide and ~1 mm deep), and demonstrated significant enhancement in the critical heat flux (CHF) of impingement boiling. However when calculated based on the total area (including the additional surface area provided by the studs or grooves), the CHF value was highest for the plain surface. They concluded that the enhancement was solely due to the additional surface area. Lay and Dhir [7] considered a free surface, cylindircal jet (diameter ~1 to 2 mm) impingement on structured surface, and demonstrated up to 2X increase in phase change heat transfer and CHF. They used several types of surface structures, such as mm scale grooves, micro-scale porous medium, and a combination of the two. Copeland [8] considered a confined, 2-D jet impingement on a micro-studded surface and studied the effect of stud width (w), varying between ~100–200 μm, and height (H) in the range of 100 μm to 1 mm.

In this context it is important to note that vast literature exists on micro and nanoscale surface modifications for phase change heat transfer enhancement in other configurations, such as pool boiling (e.g. [9]), forced convection boiling over an array of micro-pin fins (e.g. [10]), and spray impingement boiling (e.g. [11]). Since these configurations are only peripherally related to the current work, we refrain from citing the exhaustive list of literature.

All these literature conclusively prove that surface micro-structures improve heat transfer for various types of boiling including jet impingement. However, several aspects of the jet impingement boiling heat transfer on a structured surface remain unclear due to the limited literature on the topic. For example, whether the enhancement is purely due to area increase, as concluded by Wadsworth and Mudawar [6], needs a further investigation through a systematic study. The other investigators [7, 8] did not systematically quantify the area effect. Furthermore, all these previous studies [6–8] utilize a single jet, whereas most of the recent research, such as [12], [13], focus on array of jets, although on smooth surface only. The jet-to-jet interaction on the impingement surface is an important consideration for an array, and clearly the presence of surface micro-structures can alter the flow dynamics. Another distinguishing feature is the jet size. The present work considers a micro-jet of ~100 μm diameter, in comparison to Lay and Dhir's [7] ~ mm scale jet. At any radial location from the center of the jet, the liquid film thickness (t_f) on the impingement surface of a micro-scale jet is an order of magnitude lower than that for a mm-scale jet for the same jet Reynolds number (Re_j). Therefore interaction of the liquid film with the micro-structures will be different between the two cases.

In this study we investigate an array of sixteen free surface jets, each 125 μm in diameter, impinging on a micro-structured surface with a base area 1×10^{-4} m^2 (1 cm^2). Square cross-section micro-studs with characteristic size (width w) varying between 152 and 533 μm, stud height (H) varying between 51 and 152 μm, and stud spacing (S) varying between 254 and 794 μm are fabricated on the base surface. Experiments are carried out at two different jet Reynolds number (Re_j) conditions, 1012 and 1747. The study investigates the role of the micro-structure geometric parameters, and identifies an optimal structure. Three dominant physical mechanisms dictate the heat transfer: (a) surface area enhancement, (b) increase in the nucleation site density, and (c) alteration of the liquid film dynamics. Results show that the structures considerably enhance heat transfer, beyond the area effect in certain cases. Up to 78% increase in the critical heat flux (CHF) is reported.

2. EXPERIMENTAL SETUP & PROCEDURE

Figure 1 shows a schematic of the overall experimental setup. The heat source is a copper heater block where six cartridge heaters are inserted. Each cartridge, 0.0095 m diameter, is capable of delivering 600 Watts at 115 V. The cartridges are connected in parallel and are powered by a 100 V/28 Amps DC supply. Power input to the heater block cartridges is calculated based on voltage (V) measurements using a multi-meter, and current (i) measurement from the digital readout of the power supply. The base of the copper heater that interfaces with the base plate (cooling surface) is 0.01 m × 0.01 m (area 1 cm^2). A high thermal conductivity, silver filled, thermal grease is used at the interface of the heater block and the base plate. The heater block, covered by alumina silica fiber insulation, is encased in a heater assembly housing.

The base plate, also made of copper, is a 2-step structure (Figure 1) and has an overall dimension of 0.07 m × 0.07 m × 0.006 m. The shoulder of the base plate is covered with an insulating frame, made of G-10. The bottom face of the base plate on which impingement occurs, has the same cross-sectional area as the heat source, i.e. 0.01 m × 0.01 m (A_{base} = 1 cm^2). The shape of the base plate and its thickness are dictated by rigidity, robustness and interchangeability considerations of the practical application platform. The shape of the G-10 frame minimizes heat loss from the shoulder and the exposed (to air) side walls of the base plate. At the highest heat flux condition, the loss is estimated to be less than 2%. Therefore, heat flux at the cooling surface of the base plate can be considered the same as the bottom of the heater block, which is nearly iso-flux. Four 0.0012 m diameter holes are drilled on the sides of the base plate to various depths, to measure base plate temperatures using K-type (Chromel-Alumel) thermocouples.
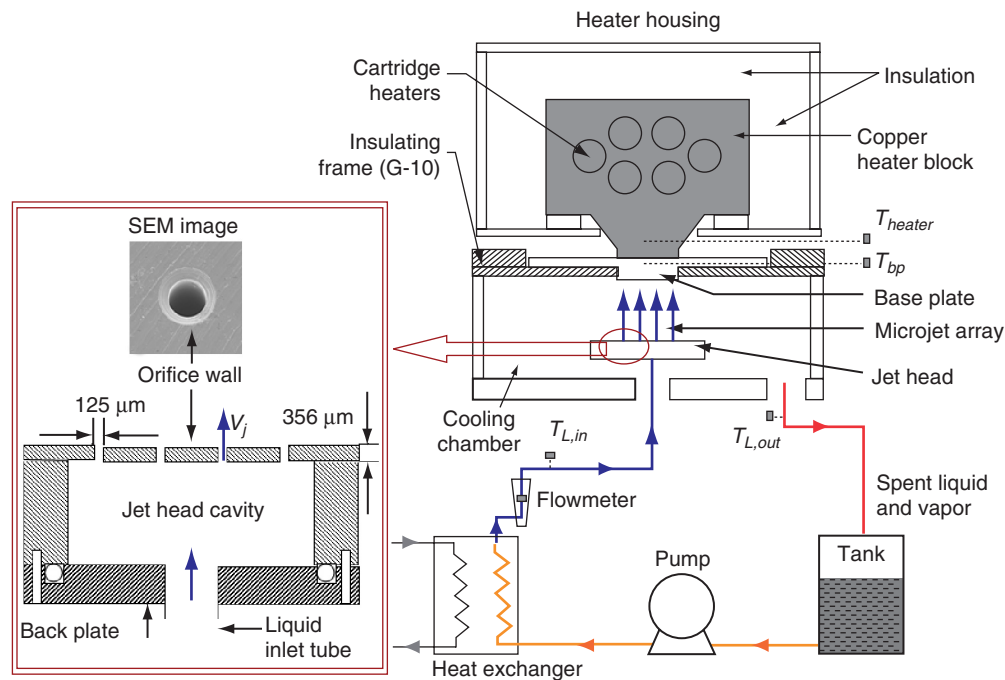
Figure 1. Schematic of the experimental setup including heater assembly, and closed loop micro-jet array impingement cooling system. A schematic of the jet head assembly and a scanning electron microscope (SEM) image of one sample orifice is also shown in the inset.

A cooling chamber (0.085 m × 0.085 m × 0.035 m) attached to the base plate, houses the jet header, the key element of the closed loop cooling system. The header is a cavity, 0.01 m × 0.01 m × 0.006 m, made of stainless steel, with openings at the top and bottom wall. The coolant (DI water) enters through the opening at the bottom wall and emerges as jets through the micro-orifices at the top wall. The top wall is 356 μm thick through which 16 (an array of 4 × 4) 125 μm diameter (D_j) micro-orifices are drilled, using a high speed (~7500 RPM) CNC machine. Note that the total orifice area ($N_j \pi D_j^2/4$) is only 0.05% of the jet head cavity area. The orifices are conformal to the drill shape, i.e. perfectly cylindrical, circular in cross-section and orthogonal over the orifice plate thickness (356 μm). The inset of Figure 1 shows a scanning electron microscope (SEM) image of the micro-orifice. The pitch (P) between the jets is 0.0025 m, i.e. $P/D_j = 20$. The current orifice size and the number of jets do not necessarily provide the optimal thermal performance. Their choice is guided by other constraints, such as availability and reliability of the micro-drills; ease and cost of manufacturing; potential of clogging in the practical application; and pressure drop in the flow loop. A 75 μm filter, less than half the diameter of the orifice, is used in the closed loop system to avoid clogging of the micro-orifices. The impingement distance between the jet header and the base plate (z) is fixed at 0.01 m. This ensures that the jets impinge as free surface (liquid in air) jets. The jets flow upwards, against gravity. Thus draining of the spent (used) liquid from the impingement surface to the bottom of the chamber, and then to the tank, is assisted by gravity. The bottom wall of the cooling chamber is slightly sloped towards the outlet port to avoid any accumulation of the spent liquid inside the chamber. A gear pump, connected to a 12 V DC motor with a nominal 26 Watts (0.035 HP) power rating is used to drive the liquid. In a typical test run, the liquid flow rate (Q_L) is pre-set at a desired level by adjusting the input power to the motor. The flow rate is measured by a rotameter, rated for 15 to 541 cc/min ($2.5 \times 10^{-7} - 9 \times 10^{-6}$ m³/s), with an accuracy of ± 2%. Typical fluctuation in Q_L during the experiment is < 4 cc/min.

During the experiment, power input to the cartridge heaters is gradually increased. At each power level, nine different temperatures, four base plates ($T_{bp1} - T_{bp4}$), the liquid inlet and outlet ($T_{L,in}$ and $T_{L,out}$), the

heater block temperature (T_{heater}) and the heater housing surface temperature at two different locations, are monitored using an automated data acquisition system. Typically with each increase/decrease in power, about 95% of the total temperature rise/drop takes place within the first 15 minutes. As an adequate precaution, at each power level, steady state temperature values are recorded about 25 minutes after changing the power input. Maximum variation in the measured temperatures is $\pm$ 0.3°C. Flow rate of the secondary cooling loop (into the heat exchanger) is periodically adjusted to maintain $T_{L,in}$ at 20°C ($\pm$ 0.2°C).

2.1. Data reduction

Heat dissipated by the impinging jet (Q_H) is less than the power input to the cartridge heaters ($V \cdot i$) due to heat losses from: (a) heater housing walls (note that although the copper heater block is covered with poor thermal conductivity insulating blanket, it is not a perfect insulation), and (b) side walls of the heater block between the heater housing and the base plate that is exposed to air (Figure 1). In the single phase heat transfer regime it is relatively simple to accurately calculate Q_H based on calorimetry, i.e. $Q_H = \rho\, Q_L\, C_P\, (T_{L,out} - T_{L,in})$, where ρ, Q_L and C_P are liquid density, flow rate and specific heat respectively, and $T_{L,out}$ and $T_{L,in}$ are the experimentally measured liquid temperature respectively at the outlet and inlet of the cooling chamber. However, calorimetry cannot be used for phase change heat transfer since a certain (not known a priori) portion of the liquid vaporizes. Traditionally Q_H in impingement boiling is estimated, either by measuring heater block temperatures at two or three different locations along the predominant heat flow path and then applying 1-D Fourier law, or from a simplified computational model that calculates heat loss (Q_{loss}) and $Q_H = (V \cdot i - Q_{loss})$. The current setup does not allow the former technique. We estimate Q_{loss} based on an extrapolation technique of the single phase data. For this purpose, the heater block and housing temperatures are measured throughout the experiment. Since Q_{loss} can be accurately estimated in the single-phase regime, first we develop a correlation relating single phase Q_{loss} with the measured heater block and housing temperatures. Then the correlation of Q_{loss} is extrapolated to higher heater block and housing temperatures, corresponding to the phase change regime. To the first order this approach is reasonable since the heat loss mechanisms remain the same (natural convection and radiation from the surfaces) at all temperatures. At the highest power level (CHF), the reported heat dissipation due to jet impingement boiling (Q_H) varies between 73 to 89% of power input ($V \cdot i$), depending on the flow rate. Based on this estimated Q_H, heat flux is reported either using the base area (A_{base}) or the total surface area (A_{total}).

At each power level and flow rate, the four base plate temperature measurements are used to calculate an average base plate temperature ($T_{bp,av} = \{\Sigma T_{bp1} + \cdots T_{bp4}\}/4$). The average temperature at the impingement surface ($T_{s,av}$) is then calculated from $T_{bp,av}$ using Fourier law of 1-D heat conduction, i.e. $T_{s,av} = T_{bp,av} - (Q_H d)/(A_{base} k_s)$, where d is the depth of the base plate step (Figure 1), and k_s is the thermal conductivity of the base plate material (copper). Based on the total liquid flow rate measurement (Q_L), Reynolds number (Re_j) for each individual jet is calculated as $Re_j = 4Q_L/(N_j\,\pi\,D_j\,\nu)$. All the property values are estimated at an average temperature, i.e. $(T_{s,av} + T_{L,in})/2$.

The experimental conditions and the corresponding calculated dimensionless parameters are listed in Table 1.

2.2. Uncertainty analysis

Based on the measurement fluctuations and accuracy of the data acquisition systems, Nth-order uncertainty of limited sample experimental data are calculated following Moffat [14]. The reported values are the best estimates of the results, and with 95% confidence level the true values are believed to lie within certain percentages of the reported values. For example: base plate temperature (T_{bp}) $\pm$ 0.8%, Flow rate (Q_L) $\pm$ 4.4%, input voltage (V) $\pm$ 1%, input current (i) $\pm$ 4.4%, jet diameter (D_j) $\pm$ 3.4%, base area dimensions $\pm$ 0.2% and micro-stud width (w) and height (H) $\pm$ 4%. The maximum uncertainties for other parameters, calculated from these measurements are: heat dissipation (Q_H) $\pm$ 2.8%, critical heat flux based on total area (CHF_{Atotal}) $\pm$ 2.5%, impingement surface temperature ($T_{s,av}$) $\pm$ 1.1%, jet velocity (V_j) $\pm$ 8.1% and jet Reynolds number (Re_j) $\pm$ 8.8%.

Table 1. Experimental conditions and corresponding range of dimensionless parameters. Water is used as the experimental liquid, with liquid inlet temperature ($T_{L,in}$) of 20°C.

Geometric parameters	Jet diameter D_j (m)	125×10^{-6} (125 μm)
	No of jets N_j	16 (Array of 4×4)
	Dimensionless jet pitch P/D_j	20
	Dimensionless separation distance z/D_j	80
	Heater base and Plain base plate (cooling surface) area A_{base} (m^2)	1×10^{-4} (1 cm^2)
	Total surface area of micro-structured surface A_{total} (m^2)	$(1.11 - 1.57) \times 10^{-4}$ Details in Table 2
Heat dissipated Q_H (Watts)		$23 - 1008$
Flow rate Q_L (m^3/s)		$1.6 \times 10^{-6} - 2.7 \times 10^{-6}$ ($95 - 163$ cc/min)
Jet velocity V_j (m/s)		$8.2 - 14.2$
Jet Reynolds Number (Re_j)		$1012 - 1747$
Sub-cooling of the inlet liquid ΔT_{sup} (°C)		80

3. MICRO-STRUCTURE DESIGN AND FABRICATION

The present work focuses on micro-studs with square cross-sectional (c/s) area, as shown in Figure 2a. The study aims to arrive at the optimal stud structure through a detailed quantitative study of various geometric parameters, such as: the stud size (width = length = w), height (H), spacing between studs (S), the number of studs (N_s) and stud pattern, i.e. in-line studs as shown in Figure 2b, or staggered studs as shown in Figure 2c, where alternate rows of studs are off-set from the neighboring row. To limit the wide choice of design parameters, certain constraints are imposed based on the application platform requirement, robustness considerations, and machining limitations. For example: (a) the application platform for which this cooling technique is developed requires stud height H to be ≤ 152 μm; (b) The stud spacing S is dictated by the diameter of the micro-end mill used to fabricate the structures in a 7500 RPM CNC machine. The smallest end mill for a reliable fabrication process is 254 μm diameter, i.e., $S \geq 254$ μm; (c) Studs smaller than 152 μm frequently chipped away during machining. Sub-mm length scales are avoided to maintain the focus on micro-studs. The stud size w is limited to 152–533 μm.

Keeping the base surface area (A_{base}) constant at 1 cm^2, the total heat transfer surface area (A_{total}) can be increased by increasing N_s for a constant w, so as to decrease S; or by increasing H for a constant S, N_s and w; or to a limited extent by increasing w for a given S. Several combinations of w, S and H can also lead to the same A_{total}. We manufactured eight different micro-structures, as listed in Table 2. The total area reported in this Table is based on rectangular surface area of the micro-stud ($A_{total} = A_{base} + 4wH \times N_s$). The close-up view of the micro-structure in Figure 2d shows a slight curvature at the base of the structure. This is deliberately created during the machining process to increase stud strength. The total surface area of the studs is actually slightly higher than reported ($4wHN_s$) due to the curvature. However considering the length scale of curvature (between 1 to 10 μm), the effect on A_{total} is nominal. Also note that the additional area of micron and sub-micron scale roughness elements is not considered in the A_{total} calculation. The plain surface (not listed in Table 2), fabricated by milling followed by lapping has an RMS surface roughness of 0.4 μm. Experiments are conducted in four different test sets:

Test set 1: Area effect through number of studs (N_s) — w and H are kept constant at 152 μm, while N_s is increased, thereby reducing S and thereby increasing A_{total}. Four different micro-structures, MS1, MS2, MS3 and MS4 (all in-line arrays), are compared with the plain surface.
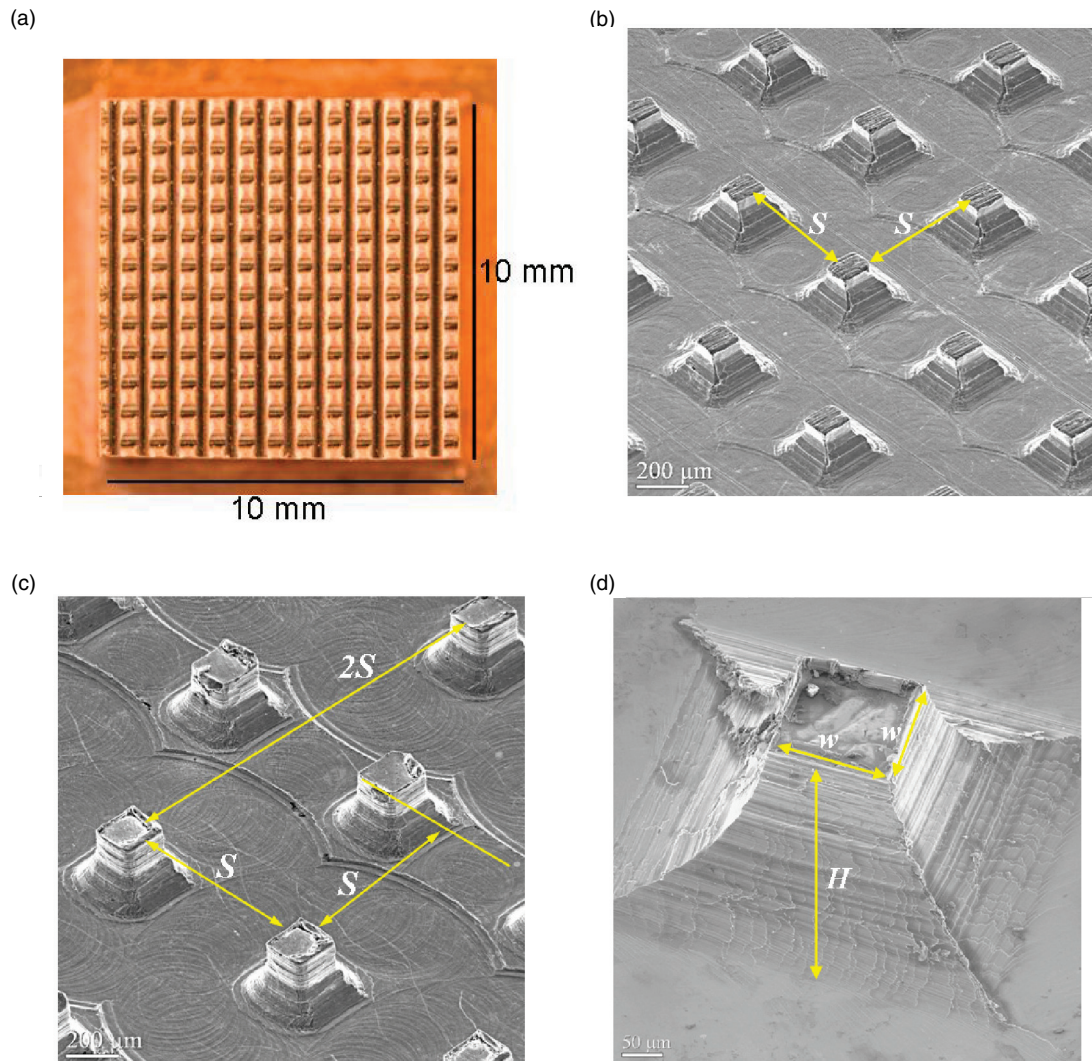
(a)

(b)

(c)

(d)

Figure 2. Images of the 1 cm^2 area base plate with micro-studs: (a) overall base plate picture, (b) an in-line micro-stud array, (c) a staggered micro-stud array, and (d) a single micro-stud.

Table 2. Geometric details of eight different micro-structure patterns (MS–MS8) considered for heat transfer enhancement.

Surface pattern	w in μm	H in μm	S in μm	N_s	(A_{total}/A_{base})	Stud pattern
MS1	152	152	794	121	1.11	In-Line
MS2	152	152	508	225	1.21	In-Line
MS3	152	152	381	361	1.33	In-Line
MS4	152	152	254	625	1.57	In-Line
MS5	279	152	635	121	1.20	In-Line
MS6	533	152	794	64	1.20	In-Line
MS7	152	51	381	361	1.11	In-Line
MS8	152	152	508	225	1.21	Staggered

Test set 2: Area effect through stud height — w, S and N_s are held constant respectively at 152 μm, 381 μm and 361, while varying H. Micro-structures MS3 and MS7 (both in-line arrays) are compared.

  Test set 3: Stud size effect — A_{total}/A_{base} and H are held constant at 1.21 and 152 μm respectively, while varying w and S. Micro-structures MS2, MS5 and MS6 (all in-line arrays) are compared.

  Test set 4: All parameters are held constant and the stud pattern is varied between in-line and staggered. Micro-structures MS2 and MS8 are compared.

4. RESULTS & DISCUSSION

The effects of jet diameter (D_j), average jet velocity (V_j), sub-cooling (ΔT_{sub}), and the separation distance between the nozzle and the target surface (z), on free surface jet impingement boiling have been widely investigated in the literature, and reviewed by Wolf et al [5]. Therefore these parameters are mostly held constant in this study, and the focus is on the impingement surface structural modification aspect. Only two different flow rate conditions (Re_j = 1012 and 1747), are investigated, just to expand the basis of conclusion of an optimal micro-structure. A combined effect of three distinct mechanisms governs the phase change heat transfer.

(1) ***Surface area***—Micro-structures act as fins and increase the total heat transfer surface area (A_{total}) by 11 to 57% compared to the plain surface, as shown in Table 2. Intuitively, that enhances heat transfer.

(2) ***Flow dynamics on the impingement surface***—The free surface micro-jets (liquid jets in air) form a thin liquid film (t_f < ~100 μm) on the impingement surface. Heat transfer is very effective in the thin film region due to high-speed liquid flow, continuous growth of small vapor bubbles underneath the film and its rupture on the liquid-air interface, and evaporation from the thin film surface. In the case of impingement on the plain surface, the impinged liquid flows unobstructed radially away from the center of the jet, until colliding with a similar flow front formed by the neighboring impinging jet. For impingement on a micro-structured surface, each micro-jet impinges on the surface in between the micro-studs, as shown in the schematic of Figure 3. The micro-studs partially obstruct the radial spreading of the fast
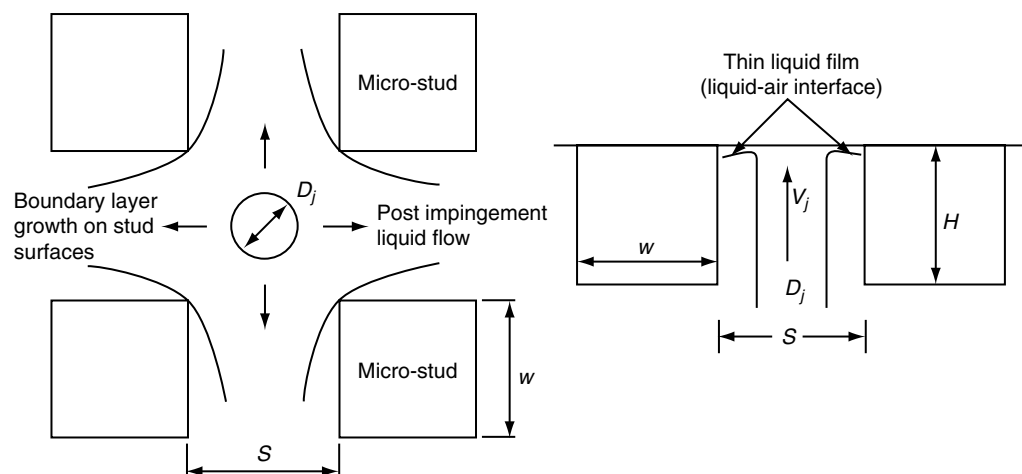

Figure 3. Schematic of liquid flow after micro-jet impingement on a micro-structured surface. The portion of the microstructure height (H) that the liquid film wets is a figurative representation. The actual wetted area depends on the flow rate and structure pattern, and is not quantified in this study.

moving thin film. As the liquid flows between the studs, the likely effect is an increase in the film thickness (t_f) and a reduction in film velocity. Both adversely affect the heat transfer over the area covered by the jet (also called the wall jet region of the impingement surface). On the positive side, formation of new velocity and thermal boundary layers at each micro-stud surface may improve heat transfer, particularly in the single-phase regime. However during impingement boiling this effect is expected to be nominal.

(3) ***Bubble nucleation site***—That the number of active nucleation sites increases with surface roughness is a well-established fact for pool boiling (e.g. [15]). The conventional machining process inherently introduces micron and sub-micron scale roughness elements on the studs, as observed in the close-up images Figure 2c and 2d. Air or vapor trapped in these elements acts as bubble nucleation sites if the structure surfaces are wet by the liquid film, thereby drastically improving the phase change heat transfer. The greater the portion of the micro-structure height covered by the liquid film, the higher the active nucleation site density.

To summarize, the micro-structures adversely affects the heat transfer in the wall jet region of the impingement surface by obstructing (at least partially) the fast moving liquid film. However, they also provide additional surface area and potential sites for bubble nucleation. In an extreme case if the spacing (S) is very small, the impinged liquid may not wet the entire available micro-structure surface area, and may instead drip or splatter away from the surface.

Test set 1—Area effect through number of studs: Phase change heat transfer due to micro-jet array impingement on a plain surface and four different micro-structured surfaces (MS1–MS4) is compared in Figure 4. Variation of the heat flux calculated over the base area of the impingement surface (Q_{Abase}) with the superheat of the average impingement surface temperature (ΔT_{sup}) is plotted in Figure 4a, for a constant flow rate ($Re_j = 1012$). Compared to the plain surface, the micro-structures lower the superheat for the onset of nucleate boiling, similar to that observed in pool boiling [16]. This is due to the increase in the active nucleation site density. Both the fully developed nucleate boiling and the critical heat flux (CHF) substantially increase from the plain surface to the
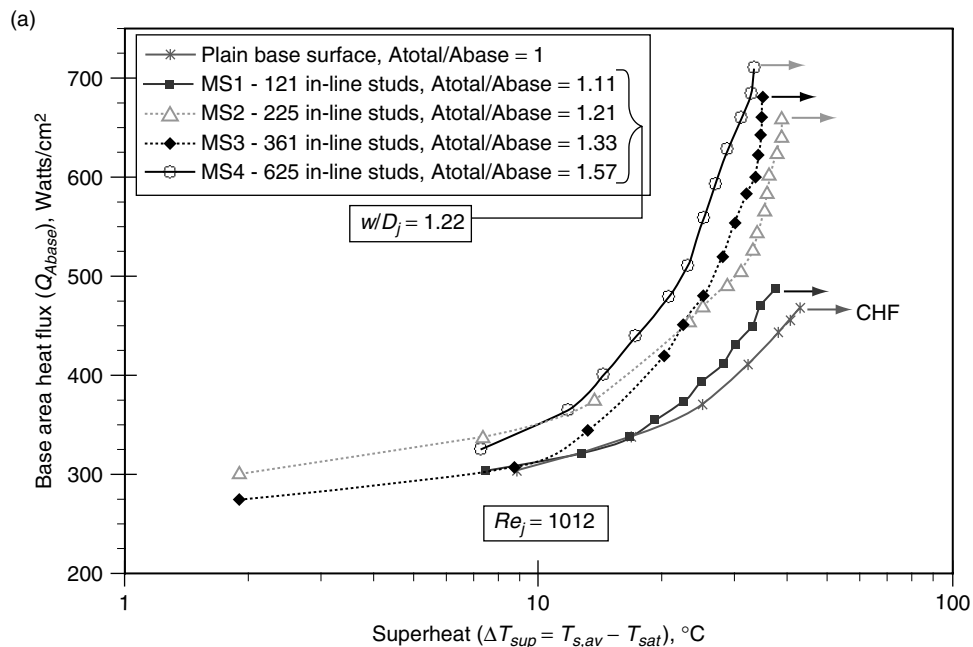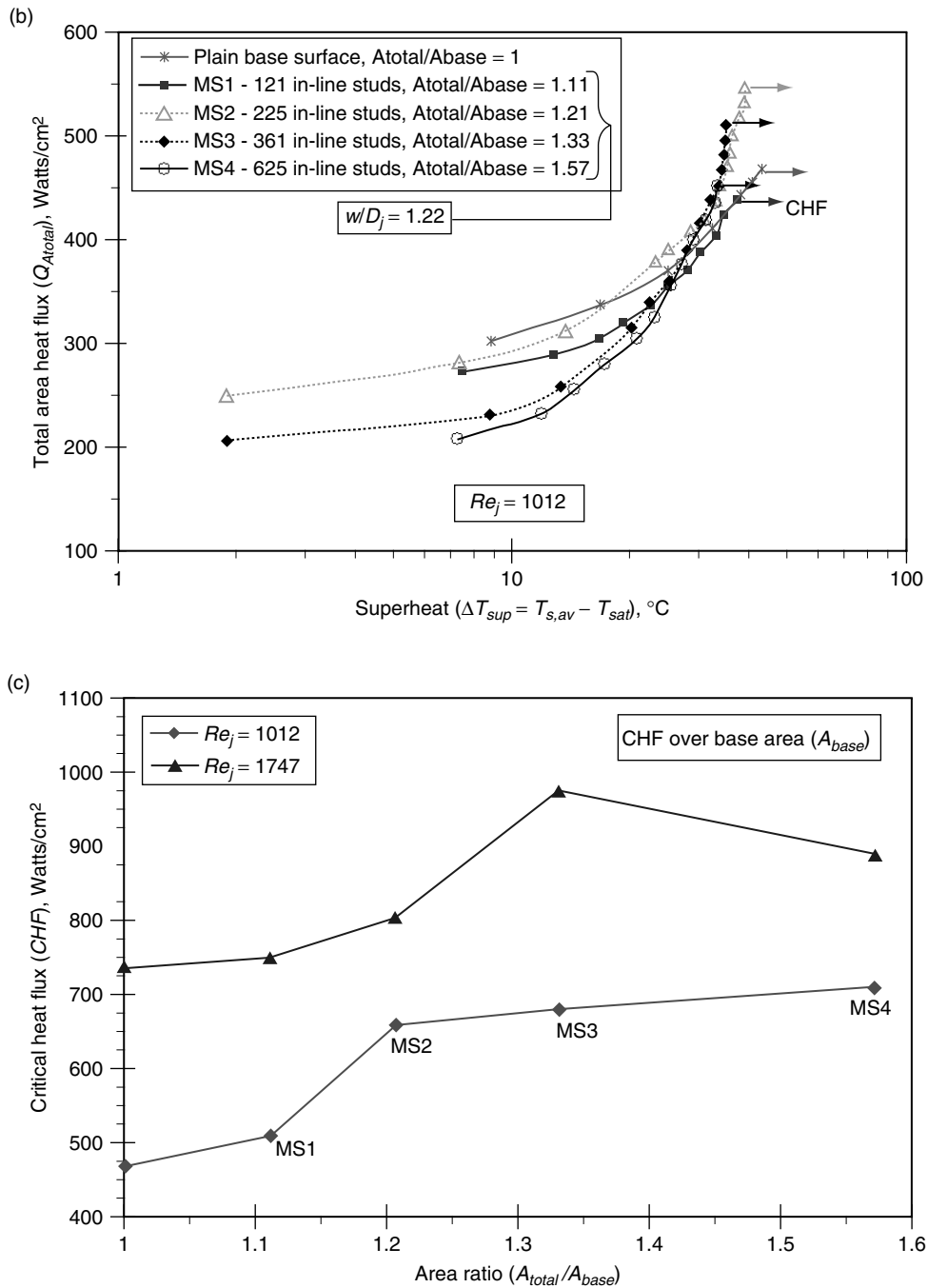

Figure 4. (*Continued*)

Figure 4. Comparison of micro-jet array impingement boiling on a plain surface and four different micro-structured surfaces (MS1–MS4). (a) Heat flux calculated over base area (Q_{Abase}, $A_{base} = 1$ cm^2) vs. superheat of the average impingement surface temperature (ΔT_{sup}) for a constant flow rate ($Re_j = 1012$); (b) Heat flux calculated over the total surface area (Q_{Atotal}) vs. superheat of the average impingement surface temperature (ΔT_{sup}) for a constant flow rate ($Re_j = 1012$); (c) Variation of the critical heat flux (CHF) calculated over the base area with area ratio (A_{total}/A_{base}) for two different flow rate conditions ($Re_j = 1012$ and 1747).

structured surfaces, as the number of studs (N_s) increase from MS1 through MS4. Clearly the positive impacts of microstructures, such as additional surface area and nucleation sites, overwhelm the negative effect of impeding the high-speed spreading of the thin film. Figure 4a also shows that the micro-structures gradually increase the slope of the impingement boiling curve. Multiple researchers have reported similar findings for pool boiling and these have been summarized by Poniewski and Thome [17].

The heat transfer enhancement from the plain surface all the way up to MS4 observed in Figure 4a could be solely due to the additional surface area, as concluded by Wadsworth and Mudawar [6]. In Figure 4b, we re-examine their conclusion by plotting heat flux calculated over the total area (A_{total}) against ΔT_{sup}. A comparison between the plain surface and MS1 curves indicates that the superior heat transfer performance of MS1 (as observed in Figure 4a), is due to the additional surface area. In fact, at a low superheat level close to the onset of boiling ($\Delta T_{sup} < \sim 20°C$), this observation is true for all the micro-structured surfaces as Q_{Atotal} for all micro-structures in Figure 4b are lower than that for the plain base surface. However, at higher superheat the benefit of a micro-structured surface goes beyond the area effect as the number of active sites for bubble nucleation dramatically increases. Even based on A_{total}, MS2 significantly outperforms the plain surface and MS1. With increasing number of studs (N_s) from MS2 through MS4, the heat transfer performance in the wall jet region degrades. The nucleation site density does not increase at the same proportion as the total area, since the impeding structures may not allow complete wetting. As a result in Figure 4b Q_{Atotal} drops beyond MS2.

Figure 4c shows the variation of the critical heat flux (CHF) calculated over the impingement surface base area ($A_{base} = 1 \text{ cm}^2$), with area ratio ($A_{total}/A_{base}$) for two different flow rate (Re_j) conditions. As expected, CHF increases with Re_j for both the plain and micro-structured surfaces. At $Re_j = 1012$, CHF always increases with area ratio, whereas for $Re_j = 1747$, CHF drops from MS3 to MS4. At higher flow rates, the liquid film is thinner and the film spreads at a higher velocity. Therefore impedance due to the presence of micro-structures is stronger. It appears that the liquid film does not flow between the dense structures in MS4. Hence the heat flux, even calculated over the base area, decreases sharply. Based on the discussion in Figures 4a and 4b, it is further noted that when CHF gradually increases from one structure to another, it is primarily due to the additional area effect. Whereas the sudden increases, e.g. between MS1 to MS2 for $Re_j = 1012$, and between MS2 to MS3 for $Re_j = 1747$, are due to higher nucleation site density, in addition to the area effect. Another important observation is that at higher Re_j condition, the sudden increase happens at a denser (higher N_s) structure. Intuitively at higher Re_j, the liquid film wets a smaller portion of the stud height (H). Therefore stronger impedance from a denser structure is necessary to increase the film thickness and activate more nucleation sites.

Test set 2—Area effect through stud height (H): Keeping w, S and N_s constant, the effect of H is investigated in Figure 5. The dimensionless stud height (H/w) is varied from 0.33 in MS7 to 1 in MS3, resulting in a dimensionless total area increase from $A_{total}/A_{base} = 1.11$ to 1.33. Heat flux calculated over both the base area and total area (Q_{Abase} and Q_{Atotal}) are plotted on the dual y axis against ΔT_{sup} for a constant Re_j of 1012. Q_{Abase} is consistently higher for the taller micro-structure. However the shorter structure has higher Q_{Atotal} at low superheat and close to the CHF region, and a nearly identical fully developed nucleate boiling region. Clearly the higher Q_{Abase} of MS3 is due to the additional area effect.

A comparison between MS1 in Figure 4a/4c and MS7 in Figure 5 shows CHF values of 486 and 656 Watts/cm^2 respectively, both calculated over A_{base} at $Re_j = 1012$. MS1 (121 studs, 152 μm tall) and MS7 (361 studs, 51 μm tall), both 152 μm wide, has the same total area ($A_{total}/A_{base} = 1.11$). Yet the performance difference arises from the number of nucleation sites. With higher number of studs, MS7 is likely to have more micro-structure surface area covered by the film activating more nucleation sites, compared to that for MS1. Although the wall jet region heat transfer is expected to be better for MS1, the additional nucleation sites more than compensates for the loss.
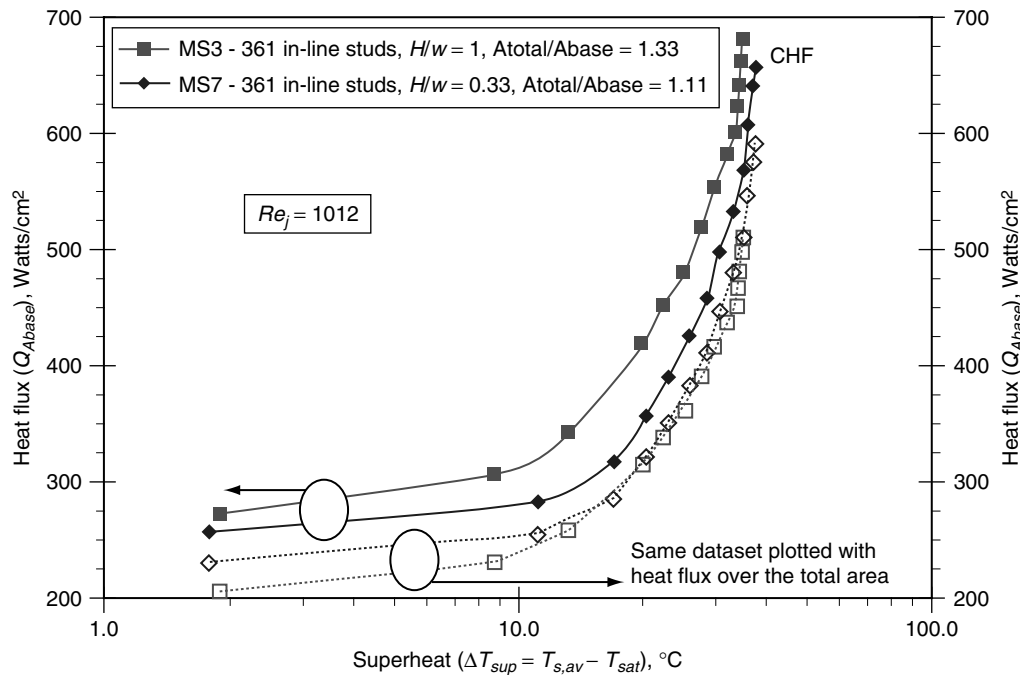
Figure 5. Effect of stud height (*H*) on micro-jet array impingement boiling on micro-structured surfaces. Heat flux calculated over base and total surface area (Q_{Abase}, Q_{Atotal}) vs. superheat of the average impingement surface temperature (ΔT_{sup}) for a constant flow rate (Re_j = 1012). Stud width (*w*) and number of studs (N_s) held constant at 150 μm and 361 respectively. Solid symbols represent Q_{Abase}, while the hollow symbols represent same heat dissipation calculated over the total area (Q_{Atotal}).

Test sets 3 and 4—Stud size and pattern effects: The effect of stud width (*w*) and pattern (in-line vs. staggered array) are investigated in Figure 6, keeping the total surface area (A_{total}) constant at A_{total}/A_{base} = 1.21. The stud height (*H*) is also held constant at 152 μm. Figure 6a shows the variation of Q_{Abase} with ΔT_{sup} for four different micro structures at a constant Re_j of 1012. As discussed earlier, the micro-structures obstruct spreading of the thin film, thereby increasing the film height, wetting more of the micro-structured surfaces and triggering additional sites for bubble nucleation. On the other hand, with fewer and far apart studs (higher *S*), the thin liquid film spreads at a faster velocity thereby improving heat transfer in the wall jet region of the impinging jets. The overall effect of the two competing mechanisms is optimal for MS5 in test set 3 (MS2, MS5 and MS6). MS5 achieves ~30% higher CHF compared to MS2. As *S* increases further from MS5 to MS6, heat transfer reduces drastically. This is due to the fact that the positive effect of high-speed thin film flow reaches a point of diminishing return. At a given velocity, the wider the area of coverage a single impinging jet (wall jet region), the less is the average heat transfer. In test set 4 staggering alternate rows of studs (as shown in Figure 2c) between MS2 and MS8 keeping every other parameter constant also leads to higher *S* and ~20% increase in CHF.

Results of Figure 6a emphasize the importance of stud spacing (*S*). Therefore, variation of CHF (calculated over A_{base}) with dimensionless *S* (S/D_j) is plotted in Figure 6b for two different Re_j conditions. MS5 shows the best performance among the four, and in fact among all the eight micro-structures investigated in this study. Compared to the plain surface MS5 achieves 37% and 78% higher CHF, respectively for Re_j = 1747 and 1012. From the trend of both the Re_j curves in Figure 6b it appears that there may be an optimal spacing between S/D_j = 4.3 (MS8) and 5.1 (MS5), where the CHF is possibly even higher.
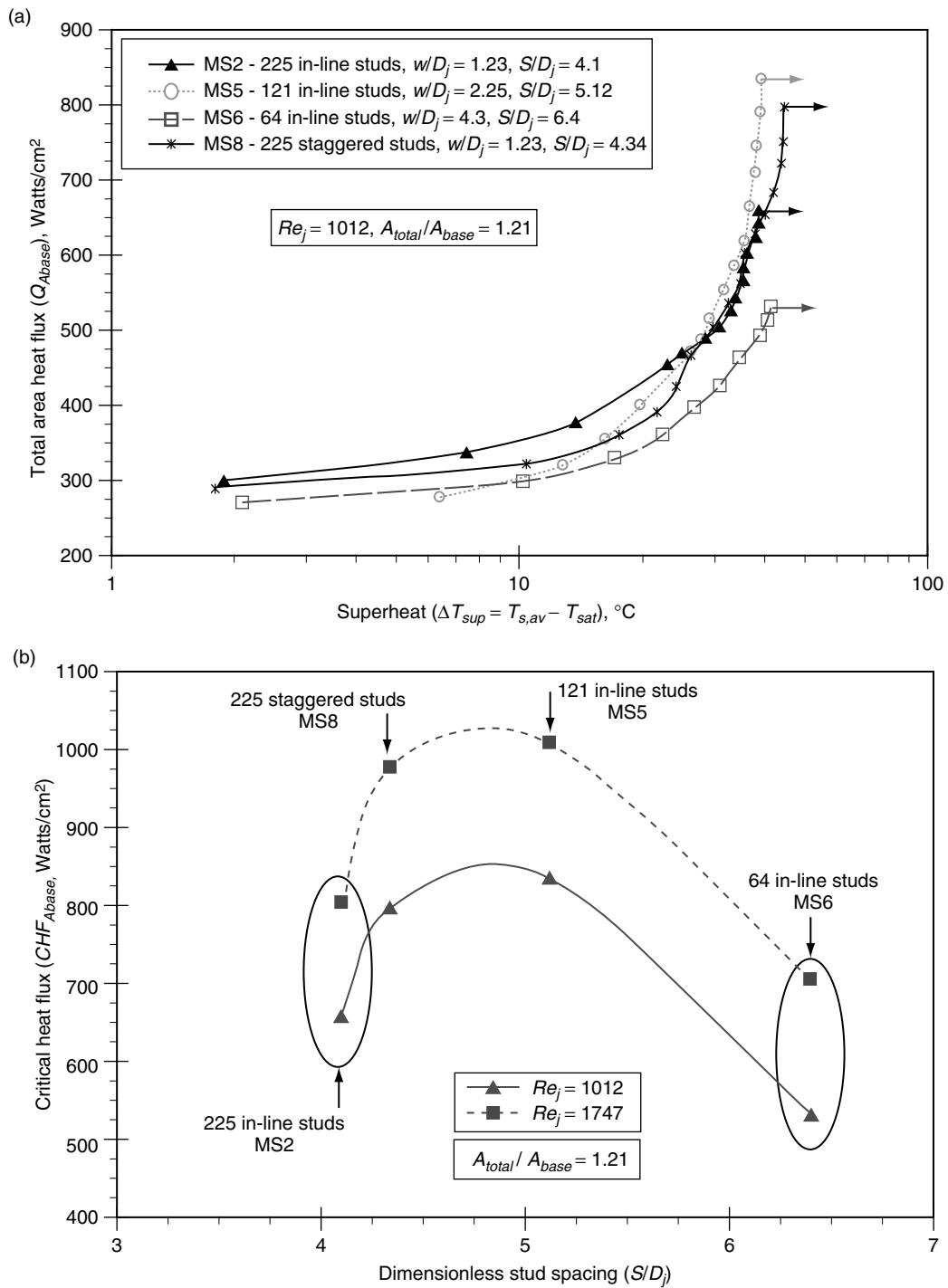
Figure 6. Effect of stud width (w) and stud pattern on micro-jet array impingement boiling on micro-structured surfaces. Total surface area and stud height are held constant, respectively at $A_{total}/A_{base} = 1.21$ and $H = 152$ μm. (a) Heat flux calculated over the base surface area (Q_{Abase}) vs. superheat of the average impingement surface temperature (ΔT_{sup}) for a constant flow rate ($Re_j = 1012$). (b) Variation of critical heat flux (CHF) calculated over the base area with dimensionless stud spacing (S/D_j) for $Re_j = 1012$ and 1747.

5. CONCLUSION

In pursuit of high heat flux cooling techniques for power dense electronics, this article investigates phase change heat transfer due to liquid micro-jet impingement on a micro-structured surface. Experiments are carried out with an array of sixteen free surface jets, each 125 µm diameter and spaced 0.0025 m apart, at two different flow rates that correspond to individual jet Reynolds numbers of 1012 and 1747. The base area of the heat source on which the impingement takes place is $0.0001\ m^2$ ($1\ cm^2$). Eight different micro-structure patterns, all square cross-sections, are explored that increase the total surface area by 11 to 57%. The stud size (width and length), height and spacing are varied between 152 to 533 µm, 51 to 152 µm, and 254 to 794 µm respectively, and two different stud patterns, in-line and staggered array are studied. Results show that the micro-structures significantly improve the impingement boiling performance compared to the plain base surface, including the onset of boiling, fully developed nucleate boiling and the critical heat flux (CHF). The performance is dictated by a combined effect of three distinct roles brought in by the micro-structures: (a) additional surface area, (b) significant increase in the number of potential sites for bubble nucleation, and (c) obstruction of the high speed spreading of the thin liquid film on the impingement surface. Therefore the performance improvement by a micro-structured surface cannot always be explained simply by the additional surface area effect, as concluded in previous studies. The optimal microstructure (among the eight different patterns investigated here) shows 37% and 78% increase in CHF compared to the plain base surface, respectively for jet Reynolds number of 1747 and 1012. Heat flux in excess of 1000 Watts/cm^2 is demonstrated with a nominal flow rate of 163 cc/min ($2.7 \times 10^{-6}\ m^3$/sec). The current systematic, parametric study conclusively proves the benefit of a micro-structured surface for micro-jet array impingement boiling. Further studies are necessary to expand the basis of this conclusion to different jet array pattern and a wider Reynolds number regime. A visualization of the post impingement flow field elucidating the wetting pattern of the structures will also be a useful future study to quantify the nucleation site density effect.

REFERENCES

[1]   Garimella S.V. et al (2008), "Thermal challenges in next-generation electronic systems", IEEE Transaction on Components & Packaging Technologies, Vol. 31, No. 4, pp. 801–815.

[2]   Lienhard V.J. (1995), "Liquid jet impingement", Annual Review of Heat Transfer, ed. C. L. Tien, Vol. 6, pp. 199–270.

[3]   Incropera F.P. (1999), "Liquid cooling of electronic devices by single phase convection", John Wiley.

[4]   Webb B.W., and Ma C.F. (1995), "Single-phase liquid jet impingement heat transfer", Advances in Heat Transfer, ed. Harnett, Irvine, Cho and Greene, Vol. 26, pp. 105–217.

[5]   Wolf D.H., Incropera F.P., and Viskanta R. (1993), "Jet impingement boiling", Advances in Heat Transfer, ed. Hartnett, Irvine, Cho and Greene, Vol. 23, pp. 1–132.

[6]   Wadsworth D.C., and Mudawar I. (1992), "Enhancement of single-phase heat transfer and critical heat flux from an ultra-high-flux simulated microelectronic heat source to a rectangular impinging jet of dielectric liquid", Journal of Heat Transfer, Vol. 114, pp. 764–768.

[7]   Lay J.H., and Dhir V.K. (1995), "Nucleate boiling heat flux enhancement on macro/micro-structured surfaces cooled by an impinging jet", Journal of Enhanced Heat Transfer, Vol. 2, pp. 177–188.

[8]   Copeland D. (1995), "Single-phase and boiling cooling of small pin fin arrays by multiple slot nozzle suction and impingement", IEEE Transaction of Components, Packaging & Manufacturing Technology, Part A, Vol. 18, No. 3, pp. 510–516.

[9]   Honda H., Takamastu H., and Wei J.J. (2002), "Enhanced boiling of FC-72 on silicon chips with micro-pin-fins and submicron-scale roughness", Journal of Heat Transfer, Vol. 124, No. 2, pp. 383–390.

[10] Krishnamurthy S., and Peles Y. (2010), "Flow boiling on micropin fins entrenched inside a microchannel – flow patterns and bubble departure diameter and bubble frequency", Journal of Heat Transfer, Vol. 132, Art 041002.

[11] Bostanci H., Saarloos B.A., Rini D.P., Kizito J.P., and Chow L.C. (2008), "Spray cooling with Ammonia on micro-structured surfaces", Proceedings of the 11th InterSociety Conference on Thermal and Thermomechanical Phenomena in Electronic Systems, ITherm 2008, pp. 290–295, Orlando, FL.

[12] Wu S.J., Shin C.H., Kim K.M., Cho H.C. (2007), "Single-phase convection and boiling heat transfer: Confined single and array-circular imping jets", International Journal of Multiphase Flow, Vol. 33, pp. 1271–1283.

[13] Browne E.A., Michna G.J., Jensen M.K., and Peles Y. (2010), "Microjet array single-phase and flow boiling heat transfer with R134a", International Journal of Heat and Mass Transfer, Vol. 53, pp. 5027–5034.

[14] Moffat R.J. (1988), "Describing the uncertainties in experimental results", Experimental Thermal and Fluid Science, Vol. 1, pp. 3–17.

[15] Dhir V.K. (1998), "Boiling heat transfer", Annual Review of Fluid Mechanics, Vol. 30, pp. 365–401.

[16] Nakayama W. (1986), "Thermal management of electronic equipment: A review of technology and research topics", Applied Mechanics Review, Vol. 39, pp. 1847–1868.

[17] Poniewski M.E., and Thome J.R. (2008), "Nucleate boiling on micro-structured surfaces", Online publication (E-book) of Heat Transfer Research Institute (HTRI): *https://www.htri.net/Public/prodsvcs/NucleateBoiling.pdf*